Supplementary Materials for

FKF1 conveys crucial timing information for CONSTANS stabilization in the photoperiodic flowering

Young Hun Song[1], Robert W. Smith[2], Benjamin J. To[1], Andrew J. Millar[2], Takato Imaizumi[1]*

*Correspondence to: takato@u.washington.edu

This PDF file includes:

Materials and Methods
Figs. S1 to S20
Tables S1
Supporting references (*20-40*)

Materials and Methods

Plant materials and growth conditions

All *Arabidopsis thaliana* plants, *fkf1-2* (*8*), *35S:HA-FKF1/fkf1 #10* (*10*), *FKF1:HA-FKF1/fkf1 #24* (*10*), *CDF1:HA-CDF1 #24* (*9*), *CDF1:HA-CDF1/fkf1-2 #29* (*9*), *SUC2:CO-HA* (*20*) transgenic lines and *cdf1-R cdf2-1 cdf3-1 cdf5-1* quadruple mutant (*14*) are in Columbia (Col-0) ecotype. The *cdf* quadruple mutant was kindly provided by Dr. G. Coupland (Max Planck Institute for Plant Breeding Research, Germany). For *35S:CDF1/ SUC2:CO-HA* transgenic lines, the full-length of *CDF1* cDNA was amplified using a forward primer (5'-CACCATGCTGGAAACTAAAGATCCTGCG-3') and a reverse primer (5'-ACGCGTCGACTCACATCTGCTCATGGAAATTGA-3') and cloned into pENTR/D-TOPO vector (Invitrogen). After verifying the sequences, *CDF1* cDNA was transferred into pB7WG2 binary vector (*21*) using LR Clonase II enzyme mix (Invitrogen) to generate *35S:CDF1*. The binary vector harboring *CDF1* overexpression cassette was introduced into the *SUC2:CO-HA* plants by conventional *Agrobacterium*-mediated transformation method. To generate *35S:CO-3F6H* and *35S:CO-3F6H 35S:HA-FKF1/fkf1* lines, we first synthesized the tandem repeats of 3 x FLAG and 6 x Histidine (3F6H) tags (5'-GATTACAAGGATCATGATGGTGATTACAAGGATCA CGACATCGACTACAAGGATGACGATGACAAGCACCATCATCACCACCATTGA -3', the sequences encoding 6 x His tag are underlined) and amplified with a 3F6H specific primer set (BamHI-3F6H forward, 5'-CGGGGATCCCAGGATCTGGTGGAG ATTACAAGGATCATG, and XbaI-3F6H reverse, 5'-GCTCTAGATCAATGGTGGT GATGATGGTGCTTGTCATCGTCATCCTTGTAGTCG-3'). The 3xFLAG-6xHis tag sequences were cloned into *BamHI-XbaI* sites of pRTL2 vector (*22*) (named pRTL2-3F6H), and the sequences were verified. Next, a *NcoI* restriction enzyme site in *CO* cDNA was mutagenized without changing amino acids by a PCR based method. The *CO* cDNA was amplified using a primer set [NcoI-CO forward, 5'-TCACCATGGTGAAA CAAGAGAGTAACG-3' and BamHI-CO reverse, 5'-CTGGGATCCCGAATGAAGG AACAATCCCATATC-3' (*CO* specific regions are underlined)] without a stop codon and inserted to *NcoI-BamHI* sites of the pRTL2-3F6H vector to make an in-frame fusion with 3F6H sequences. After confirming *CO* cDNA sequences, the *CO-3F6H* cDNA was amplified using a GTWY-CO forward primer (5'-CACCATGTTGAAACAAGAGAG TAACGACATAGG-3', *CO* specific sequences are underlined) and the XbaI-3F6H reverse primer, cloned into pENTR/D-TOPO vector, and subsequently transferred to pB7WG2 or pK7WG2 vector (*21*) to make a *35S:CO-3F6H* construct. The pB7WG2 or pK7WG2 vectors harboring *CO-3F6H* overexpression cassette were introduced in *Arabidopsis* wild type and the *35S:HA-FKF1/fkf1 #10* plants. To generate *35S:CO* and *35S:CO/fkf1-2* plants, the full-length of *CO* cDNA was amplified with the GTWY-CO forward primer and a reverse primer (5'-TCAGAATGAAGGAACAATCCCATATC CTGT-3') and cloned into pENTR/D-TOPO. After verifying *CO* sequences, *CO* cDNA was transferred to pK7WG2 binary vector (*21*). The binary vector harboring a *35S:CO* construct was introduced into *Arabidopsis* wild type and *fkf1-2* plants. To generate *35S:3HA-CO*, the nucleotide sequences encoding 3 x HA epitope tags were incorporated in the CO forward primer (5'-ATGTATCCATATGATGTTCCAGATTATGCTTATCC ATATGATGTTCCAGATTATGCATACCCGTACGACGTCCCGGACTACGCCGCA GCTGCAATGTTGAAACAAGAGAGTAACGACATAGG-3', the sequences encoding

3 x HA epitope tags are underlined). The amplified *3HA-CO* cDNA was cloned into pENTR/D-TOPO vector and transferred to pH7WG2 vector (*21*). For *CO:HA-CO* and *CO:HA-CO/fkf1-2* lines, *CO* cDNA was amplified with the CO forward primer that contain the nucleotide sequences encoding an HA epitope tag and *SacI* recognition site (5'-CTGAGCTCTGTACCCATACGATGTTCCAGATTACGCTTACCCATACGATG TTCCAGATTACGCTATGTTGAAACAAGAGAGTAACGACATAGG-3', *SacI* recognition site is underlined) and XbaI-CO reverse primer (5'-GCTCTAGATCAGAA TGAAGGAACAATCCCATATCCTGTG-3', *XbaI* recognition site is underlined), and cloned into pCR-Blunt II-TOPO vector (Invitrogen). After the sequences of *HA-CO* cDNA were verified, the *HA-CO* cDNA was excised using *SacI* and *XbaI*. The luciferase (*luc*) cDNA in the CO (2.5kb)::luc plasmid (*9*) of which the *luc* gene expression is regulated by the *CO* promoter fragment (-2389/69) was replaced by the excised *HA-CO* cDNA fragment to generate the *CO:HA-CO* construct. The *CO:HA-CO* expression cassette was cloned into pPZP221 binary vector (*23*) for plant transformation. The *CO:HA-CO/fkf1-2* line was generated by genetic cross between *CO:HA-CO* and *fkf1-2* plants. To generate *35S:3HA-CO/35S:HA-FKF1* lines, the *35S:3HA-CO* construct in pH7WG2 was transformed into *35S:HA-FKF1/fkf1 #10* (*10*) line. The transgenic plants were selected based on the expression levels of both *CO* and *FKF1*genes.

All plants were grown on soil or Linsmaier and Skoog (LS) media (Caisson) containing 3% sucrose in plant incubators (Percival Scientific or Conviron) or Conviron growth rooms at 22ºC under full-spectrum white fluorescent light (F017/950/24", Octron Osram Sylvania) with a fluence rate of 60-90 μmol m^{-2} s^{-1} in long-day (16-h light/8-h dark) conditions and 75-115 μmol m^{-2} s^{-1} in short-day (8-h light/16-h dark) conditions. For the light treatment, red or blue light was provided by red LEDs (PAR38-E27-15W42S-RD, EagleLight) or blue LEDs (PAR38-E27-45W42S-BL, EagleLight), respectively, with light intensities of 40-55 μmol m^{-2} s^{-1}. To analyze flowering time, the number of rosette and cauline leaves on the main stem were counted when the inflorescence reached to 3-5 cm high. All flowering experiments were repeated twice independently, and similar results were obtained.

Co-immunoprecipitation experiments

For analyzing *in vivo* interaction, 9-day-old *Arabidopsis* seedlings grown in long-day conditions under white light were transferred into red or blue light at dawn or continuously incubated under the white light for additional 13 hours. The seedlings were frozen in liquid nitrogen and stored at -80 ºC. For the *in planta* interaction analysis, cDNA encoding full-length *CO* without a stop codon, which was cloned in pENTR/D-TOPO vector, was transferred to the C-terminal TAP fusion binary vector pC-TAPi (*24*) to generate a *35S:CO-TAP* construct. To create HA epitope tagged LOV (amino acids 1-173), LOV+F (*10*), F+Kelch (*10*), and Kelch (*9*) domains of FKF1 constructs, we amplified the coding regions of discrete domains with forward primers containing the nucleotide sequences encoding the HA tag (ATGGCTTACCCATACGATGTTCCAGA TTACGCTGCG). The amplified cDNAs were cloned into pRTL2 vector (designated as 35S promoter driven overexpression constructs of the HA-fused FKF1 domains), and the overexpression cassettes were transferred to pPZP221 binary vector (*23*). To construct a FKF1 F-box mutant (L214A/I223A), the full-length *FKF1* cDNA was mutagenized by PCR using the primer (5'-CCGAGATAAGGCGTTATGAGCCAAAACTTGATCAGA

TGCCTGCAATATCC-3'). *35S:HA-FKF1* (*10*), *35S:FKF1-TAP* (*8*), and *35S:HA-FKF1 LOV* variants (*10*) were described previously. These overexpression constructs were infiltrated into 3-week-old *N. benthamiana* leaves as described in (*25*), and the leaves were harvested on day 3 after infiltration. For light treatment, the infiltrated *N. benthamiana* plants were subsequently incubated in a long day for one day, in the dark for one day, and in white, red, or blue light for additional 13 hours.

For co-immunoprecipitation (Co-IP) assays, all plant tissues were ground in liquid nitrogen, and protein extraction and IP procedures were performed under dim white light at 4 ºC. Proteins were extracted in Co-IP buffer [50 mM Na-phosphate pH 7.4, 150 mM NaCl, 10% glycerol, 5 mM EDTA, 1 mM DTT, 0.1% Triton X-100, 50 μM MG-132, 2 mM Na_3VO_4, 2 mM NaF, and Complete protease inhibitor cocktail tablets (Roche)] and incubated with Protein G-coupled magnetic beads (Dynabeads Protein G, Invitrogen) that captured anti-FLAG (Sigma) or anti-Protein A (Sigma) antibodies for 10 minutes. Then, the beads were washed three times with 500 μl of Co-IP buffer without MG-132, Na_3VO_4, NaF, and protease inhibitors, and precipitated proteins were eluted with 2 x SDS sample buffer at 80 ºC for 3 minutes. Fifty percents of the eluted proteins and 1.5% of the total extract as an input for protein-protein interactions in *Arabidopsis* (shown in Fig. 2 B and D) and 10% of the eluted proteins and 0.2% of total extract as an input for interactions in *N. bethamiana* (shown in Fig. 2 A, C, E, and F and fig. S4) were resolved in 9% SDS-PAGE gels. CO-3F6H, TAP-fusion (CO-TAP and FKF1-TAP), and HA-fusion (3HA-CO and HA-FKF1) proteins were detected by western blot using anti-FLAG (Sigma), anti-Protein A (Sigma), and anti-HA (3F10, Roche) antibodies, respectively.

Immunoblot analysis and protein quantification

To detect 3HA-CO protein in *CO* overexpressors, seedlings grown on LS agar media were grown in long days or short days for 10 days or transferred to red or blue light with a 16-h light/8-h dark cycle on day 10. The seedlings were harvested at each time point on day 10. Whole protein extract was extracted using the Co-IP buffer, and nuclei were isolated using CelLytic Plant Nuclei Isolation/Extraction Kit (Sigma) based on the manufacture protocol. Proteins were resolved in 9% or 12% SDS-PAGE gels for whole extract or nuclear extract, respectively, and transferred to Nitrocellulose membranes (Whatman). 3HA-CO, actin, and histone H3 proteins were detected using anti-HA (3F10, Roche), anti-actin (C4, Millipore), and anti-histone H3 (Abcam) antibodies, respectively. Immunoreactive proteins were visualized with SuperSignal West Pico Luminol/Enhanced Solution and/or SuperSignal West Femto Maximum Sensitivity Substrate (Thermo). As we used the same transgenic lines to detect the 3HA-CO protein in both whole and nuclear extract, the difference in separation of the CO protein is due to different acrylamide percentages, 9% versus 12%.

For protein quantification, a protein on immunoblotted membrane incubated in SuperSignal West Pico or SuperSignal West Pico/Femto mixture (4:1 ratio) solution was imaged by a high sensitivity cooled CCD camera system (NightOWL, Berthold). The captured image was used for quantification with the IndiGo program (Berthold). Actin or histone H3 proteins were used for normalization of a protein in whole or nuclear extract, respectively.

RNA isolation and gene expression analysis

For gene expression analyses, 10-day-old seedlings grown on LS agar plates in long days and short days were harvested at every 3 hours during a 24-h period, and were used for RNA extraction using illustra RNAspin Mini kit (GE Healthcare). To synthesize cDNA, 2 μg of total RNA was reverse-transcribed using iScript cDNA synthesis kit (Bio-Rad). The cDNA was diluted to 40 μl of water (1:4 ratio), and 2 μl of diluted cDNA was used for quantitative polymerase chain reaction (Q-PCR) using Bio-Rad real-time thermal cycler (MyiQ). Primers and PCR conditions used for *IPP2*, *CDF1*, *CO*, *FKF1*, and *FT* amplification were described previously (*9, 10, 26, 27*). *IPP2* expression was used as an internal control to normalize cDNA amount. All expression data were calculated from at least three independent biological experiments.

Chromatin immunoprecipitation

Procedures for cross-linking, isolation of chromatin, and immunoprecipitation were performed according to Bowler et al. (*28*) with minor modifications. Briefly, 1.5 g of 10-day-old seedlings were harvested in the indicated time point and infiltrated with 1% formaldehyde for cross-linking and subsequently 0.125 M glycine for stopping the cross-linking reaction. After grinding the seedlings, nuclei were isolated and lysed in Nuclei lysis buffer [50 mM Tris-HCl pH 8.0, 10 mM EDTA, 1% SDS, 50 μM MG-132, 1 mM PMSF, protease inhibitor cocktail (Roche)], and sonicated to shear DNA to approximately 500-2000 bp DNA fragments. The chromatin sample was diluted tenfold with ChIP dilution buffer [16.7 mM Tris-HCl pH 8.0, 1.1% Triton X-100, 1.2 mM EDTA, 167 mM NaCl, 1 mM PMSF, 50 μM MG-132, protease inhibitor cocktail (Roche)]. Dynabead Protein G (Invitrogen) was pretreated with anti-HA (Roche) antibody and incubated with the chromatin solution for 2-3 hours at 4 °C. Immunocomplexes were eluted after washing using low salt, high salt, LiCl, and TE buffers, reverse cross-linked at 65 ºC overnight, and treated with proteinase K that digests all proteins. Precipitated DNA was phenol/chloroform extracted, ethanol precipitated, and dissolved in 200 μl of water. Q-PCR was performed with 2 μl of precipitated DNA samples. The primer sequences used for the amplification of *FT* genomic regions designated as amplicons 1 to 17 were the following: amplicon 1, 5'-TCTGATTTGGGGTTCAAAA-3' and 5'-TCGAACTGATTCCGATTGAA-3'; amplicon 2, 5'-GGCCAACATTAGAAGAAGATTCC-3' and 5'-TCTTGACATGGAGCGAAAGA-3'; amplicon 3, 5'-CTGCGACTGCGACCTATTTT-3' and 5'-GCCACTGTTCTACACGTCCA-3'; amplicon 4, 5'-AGTGGCTGAAGTCTGAAATG-3' and 5'- CCATAGCCTAACAACTGTAGGA-3'; amplicon 5, 5'-TCCTACAGTTGTTAGGCTATGG-3' and 5'-CATTTGCACGACCAGGATAA-3'; amplicon 6, 5'-TTATCCTGGTCGTGCAAATG-3' and 5'-CAAGCGGCCATATTATGGAA-3'; amplicon 7, 5'-CCATAATATGGCCGCTTGTT-3' and 5'-TCCATACCTACCAATGTCCG-3'; amplicon 8, 5'-CGGACATTGGTAGGTATGGA-3' and 5'-CAAGGGATCCTTCAGGTTAGA-3'; amplicon 9, 5'-TCTAACCTGAAGGATCCCTTG-3' and 5'-AATTCGAAAGCGAAAACGTTC-3'; amplicon 10, 5'-GAACGTTTTCGCTTTCGAATT-3' and 5'-GAAAAAAGTAGGGTACCGCC-3'; amplicon 11, 5'-GGCGGTACCCTACTTTTTTC-3' and 5'-CTTTAACAAGATACCTCTCTCGAC-3'; amplicon 12, 5'-

GACGACAATGTGTGATGTACG-3' and 5'-GTATCATAGGCATGAACCCTCT-3'; amplicon 13, 5'-AGAGGGTTCATGCCTATGATAC-3' and 5'-CTTTGATCTTGAACAAACAGGTG-3'; amplicon 14, 5'-GGAGACGTTCTTGATCCGT-3' and 5'-GGGAGTTCAAGTGAAAGAACC-3'; amplicon 15, 5'-CCACGCTTTCCTTTTCTCTG-3' and 5'-TGCAAGAAGTTGGTGGAAAA-3'; amplicon 16, 5'-CTACAATTGTCAGAGGGAGAGT-3' and 5'-ACTACTATAGGCATCATCACCG-3'; amplicon 17, 5'-TTCTGTGCATTCAACCGATA-3' and 5'-CAGTTTTTGGGACGCAAAGT-3'. *UBQ10* (*10*), 5'-TCCAGGACAAGGAGGTATTCCTCCG-3' and 5'-CCACCAAAGTTTTACATGAAACGAA-3'. All genomic regions were amplified with an annealing temperature of 52 °C, and Q-PCR was performed by the following program: 95 °C for 120 seconds, 70 cycles of 95 °C for 10 seconds, 52 °C for 20 seconds, and 72 °C for 20 seconds. The IP efficiency (%) in each amplicon was calculated against the total input using the following equation: $0.25\times2^{(\text{Ct input-Ct ChIP})}\times100$.

Data analysis for modeling

We took advantage of the methods of Salazar et al. (*11*) to update the photoperiod response model, supplementing the published data sets used previously (*11*) with data for wild type and various mutant backgrounds from this study. The data sets retained from (*11*) were co1, co3, co8, co9, ft1, ft3, ft8 and ft9 from the wild-type background and co3fkf1, co8fkf1, ft3fkf1 and ft8fkf1 in the *fkf1* mutant background. mRNA profiles from the same biological samples share the same index numbers. These data come from our earlier publications (*8, 29*), and were used here for optimization of the new model, providing continuity with the methods used in (*11*). Hence, the newly-obtained data for *CO* and *FT* mRNA in wild-type plants can be used to validate the new model. The new wild-type control data are strikingly similar to the older data sets (fig. S12), despite their generation by different experimentalists in a different institution, after a 9-year interval. This provides justification for testing the model against data acquired in the same experiments from mutant backgrounds.

To provide further continuity with previous studies, namely (*11*) and (*8*), the newly acquired waveforms of *CO* and *FT* mRNA in all backgrounds were normalized. *CO* mRNA data was normalized to its short-day peak in wild-type plants, whilst all *FT* mRNA data was normalized to its long-day peak in wild-type plants. In a similar manner to (*11*), a common internal standard was then used to normalize the mRNA data from all experiments (new and published), namely the maximum level of the *CO* mRNA waveform in data series co9 (one example of wild type in short days), which was set to 1.

Further to the *CO* and *FT* mRNA waveforms obtained in this study, *CDF1* mRNA and protein levels were measured, since these are components of the system to be added in the updated model. *CDF1* mRNA and protein has been shown to have a circadian rhythm (*9, 14*) (fig. S19). Although clock components, such as CIRCADIAN CLOCK ASSOCIATED 1 (CCA1), LATE ELONGATED HYPOCOTYL (LHY) and members of the PSEUDO-RESPONSE REGULATOR (PRR) family, have been shown to have a function in regulating *CDF1* mRNA (*26*), its detailed transcriptional regulation is not yet clear. Likewise CDF1 protein is regulated by members of the blue-light regulated FKF1 protein family (*14*). Rather than introducing hypothetical regulators and the inevitable

unknown parameters, we follow (*11*) in using experimental data on the *CDF1* mRNA profile as an input to the model. Data on *CDF1* were acquired in wild type, *fkf1*, *35S:CO*, *35S:CO fkf1* and *35S:CDF1 SUC2:CO* lines, whereas CDF1 protein levels were obtained in wild type and *fkf1* plants (fig. S19). FKF1 protein levels were used as another input to the system, as in models 3F1 and 3F2 in (*11*), to avoid hypothetical regulators of FKF1.

In a similar manner to *CO* and *FT*, *CDF1* mRNA waveforms were normalized to the long-day peak of *CDF1* to be used as one of the system inputs. As seen in fig. S19, *CDF1* waveforms are relatively unchanged in all backgrounds other than *35S:CDF1*. Thus, wild-type *CDF1* was used as the input to the system in all cases other than when simulating the *35S:CDF1 SUC2:CO* line. We obtained comparable CDF1 protein waveforms in short days and long days in this study, by normalizing all protein data to the FKF1 levels of the same samples, specifically the maximum of the wild-type levels of FKF1 in long days (fig. S19D). Similarly, by obtaining data that compared the peaks of CDF1 protein in wild type and *fkf1*, we estimated the relationship of CDF1 protein levels between these two backgrounds. The normalized data were used to constrain the model, as described below.

Model derivation

1. Revised connection of the circadian clock to CO

The previous photoperiod sensor model used a published model of the circadian clock to generate rhythmic *CO* mRNA expression (*11, 30*). Experimental data on FKF1 protein levels formed an input to the model, which generated the FKF1-dependent shoulder around ZT13 in long days. The second, night-time peak of *CO* mRNA was controlled by the rhythmic TIMING OF CAB EXPRESSION 1 (TOC1) protein generated by the clock model (*8, 11*). The double regulation of *CO* mRNA represented the repression of *CO* expression by CDF1, modulated by the FKF1 and GI protein complex that forms in a light-dependent manner with a further FKF1-independent role for GI, as validated experimentally (*10, 11, 14*). By using quantitative experimental data for *CDF1* mRNA (fig. S19), our updated model described this system with greater biological accuracy.

A rhythm persists in *CO* mRNA in a *gi cdf1-R cdf2 cdf3 cdf5* mutant background that would not occur if *CO* was solely regulated by CDFs (*14*). In wild type and *fkf1* plants, this is reflected in the night-time peak of *CO* mRNA. This peak has no effect on *FT*, because any CO protein produced in darkness is rapidly degraded (*31-33*). We used a component from the circadian clock in equation 1 to maintain this CDF1-independent rhythm, as before (*11*), in this case activation by TOC1 (*30*).

2. Revised regulation of CO *protein and FT transcription*

The data published in this study show two further developments to the flowering time system. First, the CO protein is stabilized before dusk by FKF1, altering the waveform of *FT* mRNA (Fig. 3). Second, CDF1 is able to disrupt the CO-dependent activation of *FT* transcription by binding to a similar region of the promoter (Fig. 1). Data from the *35S:CDF1 SUC2:CO* double overexpressors and the *35S:CO fkf1* mutant lines show that sufficient CDF1 can suppress *FT* activation even by strongly-overexpressed CO, supporting the choice of a multiplicative interaction among these regulators to control *FT* in the model (equation 4). This result also shows that transcriptional activation of *FT* is

very largely, but perhaps not completely, sensitive to inhibition by CDF1. Hence, according to the model proposed here, FKF1 has a dual role in regulating *CO* mRNA via modulation of CDF1 protein (equations 1 and 2) and *FT* mRNA (equation 4) by stabilizing CO protein (equation 3), as depicted schematically in Fig. 4A. CONSTITUTIVE PHOTOMORPHOGENIC 1 (COP1) and SUPPRESSOR OF PHYA-105 (SPA) E3-ubiquitin-ligase complex degrades CO protein especially in the dark (*31-33*). Under light, the COP1-SPA activity is suppressed by blue-light photoreceptor cryptochromes (*17, 34, 35*). Thus, the CO protein degradation rate is high in darkness, as it is destabilized by the COP1-SPA complex (*31-33*). Therefore, the phase of FKF1 has a relationship with the phases of the external environment (e.g. light) and also determines the phases of *CO* and *FT* mRNA that are internally coincident to FKF1 (*36*). *FT* mRNA transcription depends almost completely on CO protein, and is modeled to ensure that there is no *FT* mRNA in the *co* mutant background, as seen in previous studies (*37*).

The updated flowering time model equations are:

$$\frac{dc_{CDF1}}{dt} = p_1 c_{CDF1}^{(m,D)} - p_2 L c_{FKF1}^{(D)} c_{GI} c_{CDF1} - m_1 c_{CDF1} \qquad 1)$$

$$\frac{dc_{CO}^{(m)}}{dt} = B_{CO} + n_1 \frac{g_1^a}{g_1^a + c_{CDF1}^a} \frac{c_{GI}}{g_2 + c_{GI}} + n_2 \frac{c_{TOC1}^b}{g_3^b + c_{TOC1}^b} - m_2 c_{CO}^{(m)} \qquad 2)$$

$$\frac{dc_{CO}}{dt} = p_3 c_{CO}^{(m)} - p_4 \left(m_3 + m_4 D - L \frac{c_{FKF1}^{(D)}}{g_4 + c_{FKF1}^{(D)}} \right) c_{CO} \qquad 3)$$

$$\frac{dc_{FT}^{(m)}}{dt} = \left[n_3 + n_4 \frac{g_5}{g_5 + c_{CDF1}} \right] \frac{c_{CO}^c}{g_6^c + c_{CO}^c} - m_5 c_{FT}^{(m)} \qquad 4)$$

where p_i represents translational modulation; m_i are the degradation rates; n_i describes transcription rates; g_i are the Michaelis-Menten constants interpreted as binding affinities; a, b and c are the Hill coefficients; B_{CO} is the basal transcription rate of *CO* mRNA; L and D represent light and dark from the light function present in the clock model, connecting the system to the photoperiod. Superscript (D) signifies components of the model that are read into the system directly from experimental data and superscript (m) represents those components that are mRNA.

Computational methods

As with many other mathematical models of gene regulatory systems, the full set of kinetic parameters has not been measured through experimentation. Parameters can be approximated or constrained from the data sets, within biochemically reasonable bounds. High-quality timeseries from multiple genotypes and environmental conditions provide the strongest constraints, and are therefore crucial to build and then test the model. The resulting model parameters are not uniquely specified but remain extremely useful to illustrate the system's dynamics and to provide mechanistic predictions. The precision of those predictions will vary according to their parameter-dependence (as we illustrate below).

The *CO* and *FT* mRNA equations were fitted to the same published data sets that were used in the optimization of the original flowering time model (*11*). In order to determine the relationship between the parameters n_1 and n_2, representing the two rhythmic components of *CO* transcription, we fitted the *CO* mRNA equation to data from both wild-type plants and *fkf1* mutants. This ensured that the CDF1 term did not dominate the *CO* mRNA equation. In a similar manner, to obtain the correct relationship between p_2 and m_1, the CDF1 protein equation has to be fitted to data from wild type and *fkf1*. The three Hill coefficients were set to 2, representing dimeric binding of the transcriptional regulators. Another constraint that we placed on the system was that $g_4 = 3g_1$ since the binding efficiency of CDF1 protein to the promoter of *FT* appears to be ~33% as efficient as binding to the *CO* promoter [compare Fig. 1 to (*10*)], though other ratio's could be chosen without greatly affecting the model. Due to its very low abundance, we lack quantified data for CO protein in the wild type; parameter values for equation 3 were obtained by fitting equation 4 to *FT* mRNA data. In total, this meant that 18 parameters were fitted to 96 data points from the 12 wild-type and *fkf1* data sets taken from (*11*). To validate the model, the remaining 44 data sets were used that consisted of 352 data points. The resulting parameter values are given in Table S1.

The models were optimized using the simulated annealing algorithm simulannealbnd that is part of the Matlab Optimization Toolbox for Matlab R2008b (Mathworks, Cambridge, UK). Simulated annealing is able to find local optima for the models parameter set, the principles of which have recently been reviewed in (*38*). For this study we have used the slower Boltzman annealing procedure with an exponential 'temperature' update starting at an initial 'temperature' of 1. Goodness of fit was calculated by a Euclidean difference/norm that we term the "cost" of the parameter set, hence a lower cost gives a better-fitting model. When each of the obtained parameter values was increased or decreased by 10%, the changes caused moderate increases in the goodness-of-fit of *FT* simulations under long-day conditions and no significant decreases in goodness-of-fit, illustrating the robustness of the model to individual parameter changes (fig. S20).

Comparison to the previous photoperiod response model

In comparison to the previous flowering time model [termed 3F2 in (*11*)], the new mathematical model significantly improves the biological realism of the flowering time system by modeling the biochemical mechanisms of FKF1 action, which were absent from the earlier model. The simulations from the updated flowering time model for wild type CDF1 protein, *CO* mRNA, CO protein and *FT* mRNA are shown in fig. S12. Importantly, *CO* mRNA maintains the shoulder at ZT13 that was captured in the previous model (*11*). This new system also provides a slightly better quantitative fit to all of the wild-type data sets used in this study when compared to the fit of model 3F2, which was created specifically to fit a single dataset under long-day conditions, as described (*11*).

The *CO* mRNA present in the day determines the amount of CO protein produced, whereas CO protein is unstable in darkness, so it was important that the previous flowering model simulated the loss of the 'FKF1-dependent' shoulder of *CO* mRNA in an *fkf1* mutation. The CDF1- and TOC1-mediated regulation of *CO* in this model also did so, albeit with a slight delay in the shoulder at ZT13 (discussed below). It also ensured a good match to *CO* mRNA data at the subsequent dawn (*8, 11*) (fig. S13).

Describing transgenic misexpression

One of the advantages of the new model is the flexibility to incorporate further mutations to the system. As part of this study, data was collected from *CO* overexpression lines in wild type, *CDF1* overexpression and *fkf1* backgrounds (see Figs. 1 and 3). To describe *CO* overexpression, the basal transcription rate (parameter B_{CO}) was increased to 150 times its normal value. As seen in fig. S19C, the level of *CDF1* mRNA in the *CO-ox*/*CDF1-ox* background is greatly increased compared to the other backgrounds. Hence, to describe the *CO-ox*/*CDF1-ox* double overexpression line, the input $c_{CDF1}^{(m,D)}$ was changed from the wild type to the data from the *35S:CDF1 SUC2:CO* line. The *CO-ox*/*fkf1* can then be simulated by setting $c_{FKF1}^{(D)} = 0$. From figs. S14 and S15, the model simulations of *CO* and *FT* mRNA in all these backgrounds are qualitatively very similar to the experimental curves present in Figs. 1 and 3 of the study. Simulated *35S:CO* activates *FT* to higher levels and with a high baseline (fig. S15F), which still gains a marked end-of-day peak in long days, matching the data of Fig. 3B. The model shows how this follows from the rhythmic stabilization of the CO protein by FKF1 (fig. S15D). In contrast, the simulated *FT* transcription profile in *35S:CO fkf1* simply increases in the light and falls in darkness (fig. S15, E and F; compare to Fig. 3B), reflecting only light regulation of CO protein. In order to simulate the *FKF1-ox* lines, the input $c_{FKF1}^{(D)}$ was set to be at the maximum value (or twice the maximum value) throughout the diurnal cycle (fig. S18B). Comparing figs. S17 and S18 shows that our model accurately predicted the altered profile and increased level of *FT* mRNA expression under long days with increased levels of FKF1 in *CO-ox/FKF1-ox*.

Estimating the importance of FKF1 in the model

We measured the importance of the multiple roles of FKF1 by calculating the area under the curve of *CO* and *FT* mRNA over a complete cycle in long days (CO_{AREA} and FT_{AREA}), in simulations that altered only one or a subset of molecular mechanisms, in ways that would be difficult to achieve experimentally. By creating a hypothetical partial *fkf1* mutant that only lost the ability to degrade the CDF1 protein regulating *CO,* we saw that CO_{AREA} is ~74% of the wild type, whilst FT_{AREA} decreased by ~11% and led to ~12% decrease of *FT* mRNA levels at the end of the day. Similarly, the removal of the FKF1 degradation of CDF1 in the regulation of *FT* led to a decrease of ~13% in FT_{AREA} and ~10% decrease of *FT* at the end of the day. Combining these partial mutants [designated as Δ (1), Fig. 4D] led to a ~22% decrease in FT_{AREA}. By removing the stabilization of CO protein by FKF1 [Δ (2)], we observed a ~51% decrease of FT_{AREA} and ~58% less *FT* mRNA at the end of the day (Fig. 4D). Thus, the removal of FKF1 from either the degradation of CDF1 protein or from the stabilization of CO protein has a significant effect on *FT* expression, indicating that both mechanisms likely contribute to flowering time.

The decrease of FT_{AREA} from Δ(1) and Δ(2) reflect the relative importance of FKF1 action through degradation of CDF1 and stabilization of CO, respectively. To test the generality of this conclusion, we calculated FT_{AREA} in the partial mutants for 500 quasi-random parameter sets selected from a Sobol series (fig. S16). Parameter sets were scored for the goodness-of-fit of their simulations to the training data (*CO* and *FT* mRNAs, and

CDF1 protein), and those that also predicted a larger FT_{AREA} in *CO-ox/fkf1* than *CO-ox/CDF1-ox*, as had been observed in the data (Figs. 1C and 3B), were retained. From the resulting analysis, the vast majority of parameter sets had a larger FT_{AREA} in $\Delta(1)$ than $\Delta(2)$, and correspondingly had a greater maximum level of long-day *FT* expression (fig. S16). Thus the CO stabilization mechanism has a significant effect in all parameter sets that describe the training data.

As has been seen in previous studies, FKF1 protein is regulated by light signaling and the circadian clock, suggesting that this component could contribute an external coincidence module to the photoperiod sensor (*8, 10*). In this system, the circadian regulation of FKF1 expression is crucial. Hence, we hypothesized that if we removed the circadian regulation of FKF1 (such that FKF1 activity is only regulated by light) in its role as a stabilizer of CO protein, we may see altered *FT* mRNA levels during the day. We obtained this effect by setting FKF1 to a constant level in the CO protein equation throughout the whole 24 hour cycle. The effects of this change can be seen in fig. S17 where FKF1 is constantly at its maximum level, resulting in higher levels of stabilized CO protein and, thus, higher levels of *FT* mRNA. By calculating FT_{AREA}, we saw that the FT_{AREA} in short days (FT_{AREA}^{SD}) was ~46% of FT_{AREA}^{LD} under these constant-FKF1 conditions. In comparison, in a wild-type background, FT_{AREA}^{SD} is only ~23% of FT_{AREA}^{LD}. Hence, the circadian regulation of FKF1 is important for the correct timing of CO protein stabilization. In particular, it maintains low activation of *FT* in short days, preventing premature floral induction.

Limitations in the data and model, and model-derived hypotheses

The present study has experimentally validated a major prediction of our earlier model, the effect of FKF1 on *FT*, by not only acquiring the data suggested but also providing two specific molecular mechanisms. Several of the other limitations listed in (*11*) still apply, however. We note above the unknown rhythmic regulator of *CO* that must generate the night-time peak that remains in the *fkf1* mutant (*11*). A limitation of the new system is the limited understanding with regards to the circadian regulators of FKF1 protein and *CDF1* mRNA, leading us to represent them from experimental data rather than with hypothetical regulators (fig. S19). The model suggests that these components are key mediators between the circadian clock and CO. In order to produce a complete model of flowering, one would need to model the regulation of FKF1 and CDF1 such that there is no need to use data as inputs to the system. The data will need high time resolution. For example, the observed rise of *CO* mRNA in the FKF1-dependent shoulder is almost coincident with the rise in *FKF1* mRNA, as we noted previously (*11*), indicating that FKF1 acts quickly.

A further limitation is the lack of quantified data on the low-abundance CO protein in the wild type under a range of light conditions. Previous studies have shown that CO protein is regulated by phytochrome and cryptochrome photoreceptors whilst also being regulated by COP1 and the FKF1 stabilization presented here (*6, 32, 33*). In addition to its peak at the end of the day, CO protein levels can also peak just after the transition from dark to light (within half an hour after dawn). This is very marked in the *35S:CO* lines (Fig. 3). It is simulated to a lesser extent in the model, even in the wild type (fig. S12F), owing to the significant level of *CO* mRNA still present at dawn in long days

(Fig. 4B). Several studies have shown significant *FT* activation around ZT4 in wild type plants, presumably due to this CO peak, as we noted previously (*11*). FKF1 levels are low at this time, so another light-dependent regulator of protein degradation is presumably involved, as recently proposed (*6, 39*).

The new formulation of the model allows more flexibility in developing the model further and adapting the system to describe future data sets. Other known components that play a role in flowering (such as further members of the CDF and LOV domain protein families, as well as COP1) could be readily incorporated, based on data analogous to those presented here, to allow quantitative analysis in areas of the system where current understanding is incomplete.

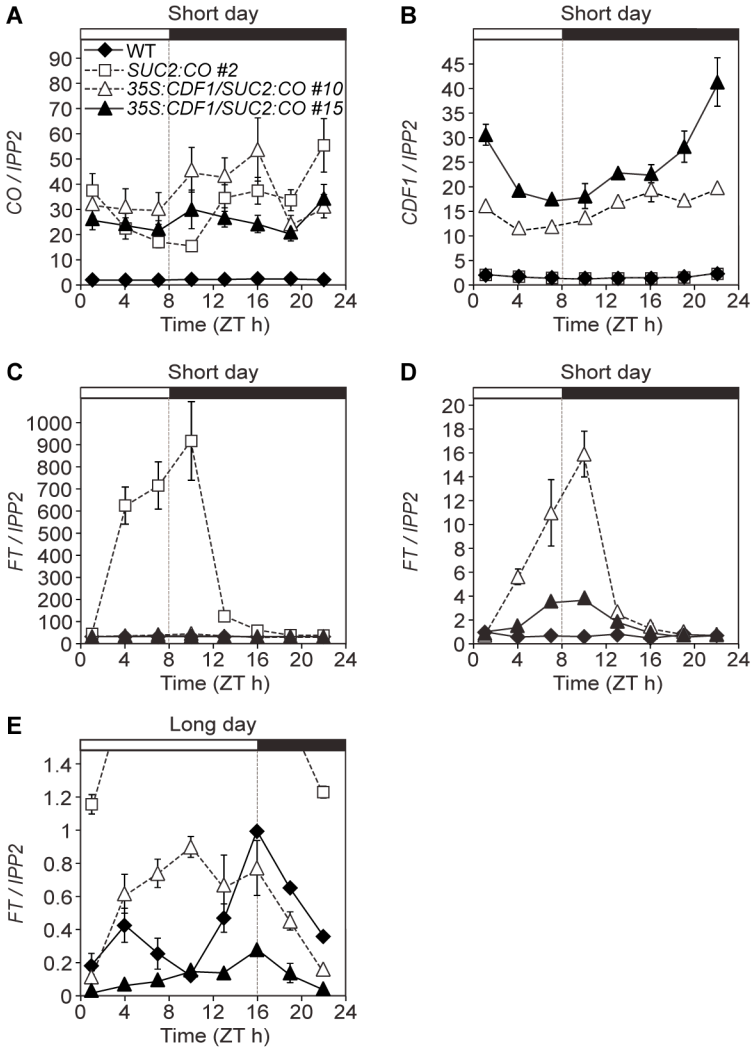

Fig. S1.
Gene expression analysis for *CO*, *CDF1*, and *FT* in long-day and short-day conditions. (**A** to **E**) wild type (WT), *SUC2:CO-HA #2*, and *35S:CDF1/SUC2:CO-HA #10* and *#15* seedlings grown in long days (**E**) or short days (**A** to **D**) were harvested on day 10. The gene expression levels of *CO* (**A**), *CDF1* (**B**), and *FT* (**C**, **D**, and **E**) were quantified by Q-PCR. (**D** and **E**) *FT* mRNA expression in WT, *35S:CDF1/SUC2:CO-HA #10,* and *#15* is shown. All expression data are shown relative to the peak expression values of each gene in WT. The results are means ± SEM from three independent biological replicates.

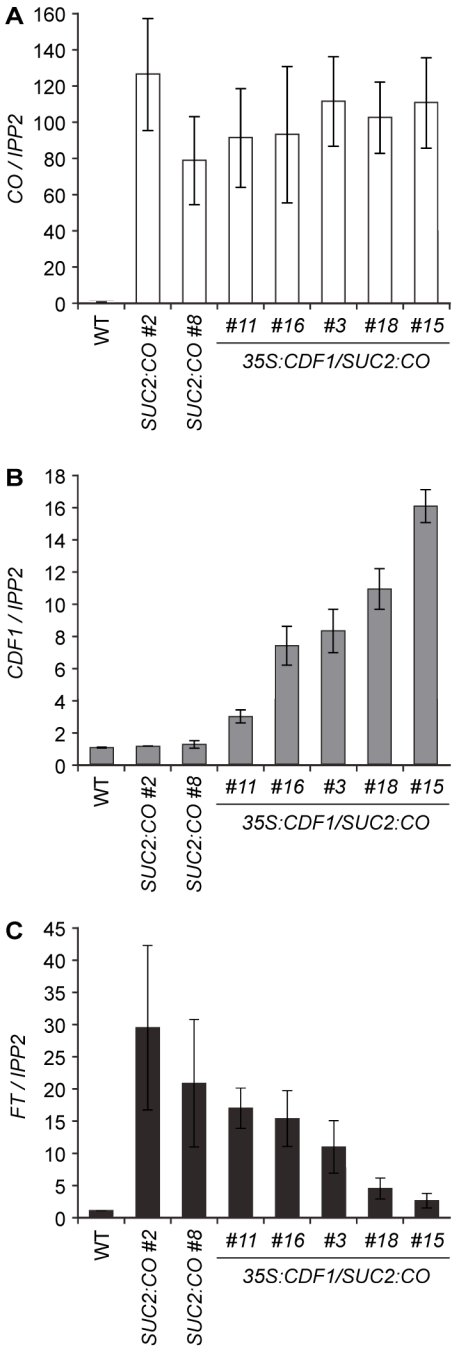

Fig. S2.
CDF1-dosage dependent repression of *FT* transcription. Two *SUC2:CO-HA* and five independent *35S:CDF1/SUC2:CO-HA* transgenic lines were grown for 10 days in long days and harvested in the morning (ZT4). (**A** to **C**) *CO* (**A**), *CDF1* (**B**), and *FT* (**C**) mRNA levels were determined by Q-PCR. The *SUC2:CO-HA* #2 was used as a parental line to generate these *35S:CDF1/SUC2:CO-HA* lines. *FT* mRNA expression levels in the *35S:CDF1/SUC2:CO-HA* lines were lower when *CDF1* mRNA levels were higher, indicating CDF1 protein represses *FT* expression in a dosage dependent manner. All

expression data are shown relative to the peak expression values of each gene in WT. The results are means ± SEM from three independent biological replicates.

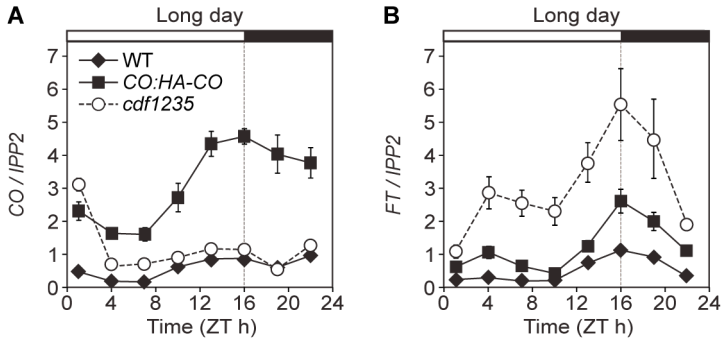

Fig. S3.
Gene expression analysis for *CO* and *FT* in wild type, *CO:HA-CO*, and *cdf1235* plants in long days. (**A** and **B**) All plants were grown for 10 days in long days. The gene expression levels of *CO* (**A**) and *FT* (**B**) were quantified by Q-PCR. All expression data are shown relative to the peak expression values of each gene in WT. The results are means ± SEM from three independent biological replicates.

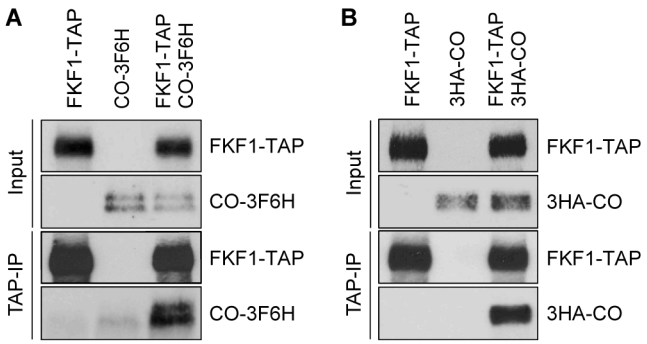

Fig. S4.
Interactions between FKF1 and CO *in planta*. Various *FKF1* and *CO* constructs were infiltrated into *N. benthamiana* for Co-IP experiments. The FKF1-CO binding was analyzed when FKF1-TAP protein was coexpressed with CO-3F6H (**A**) or 3HA-CO (**B**) proteins, indicating a protein complex between FKF1 and CO was formed in *N. benthamiana* and confirming the interaction shown in Fig. 2A.

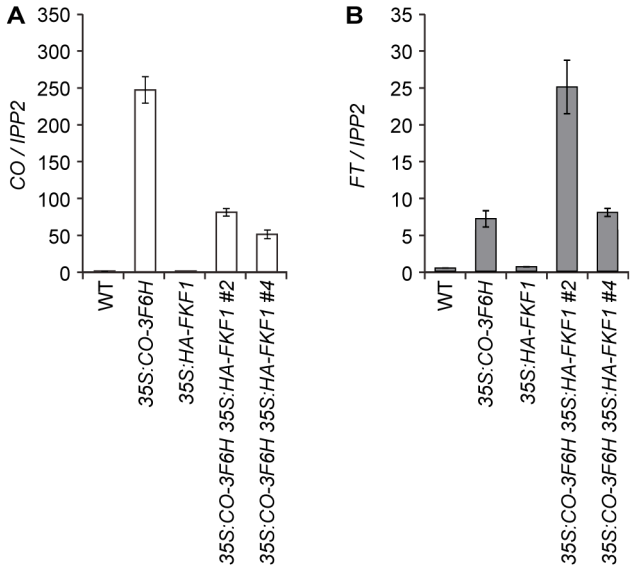

Fig. S5.
Gene expression levels of *CO* and *FT* in *CO* overexpression lines. (**A** and **B**) Wild type, the *35S:CO-3F6H* line, the *35S:HA-FKF1* line (*10*), and the *35S:CO-3F6H/35S:HA-FKF1 #2* and *#4* lines were grown in long days for 10 days and harvested at the end of the day (ZT16). Q-PCR was performed for *CO* (**A**) and *FT* (**B**) mRNA expression to confirm that the *CO-3F6H* gene is functional in *Arabidopsis*. The results are means ± SEM from three independent biological replicates.

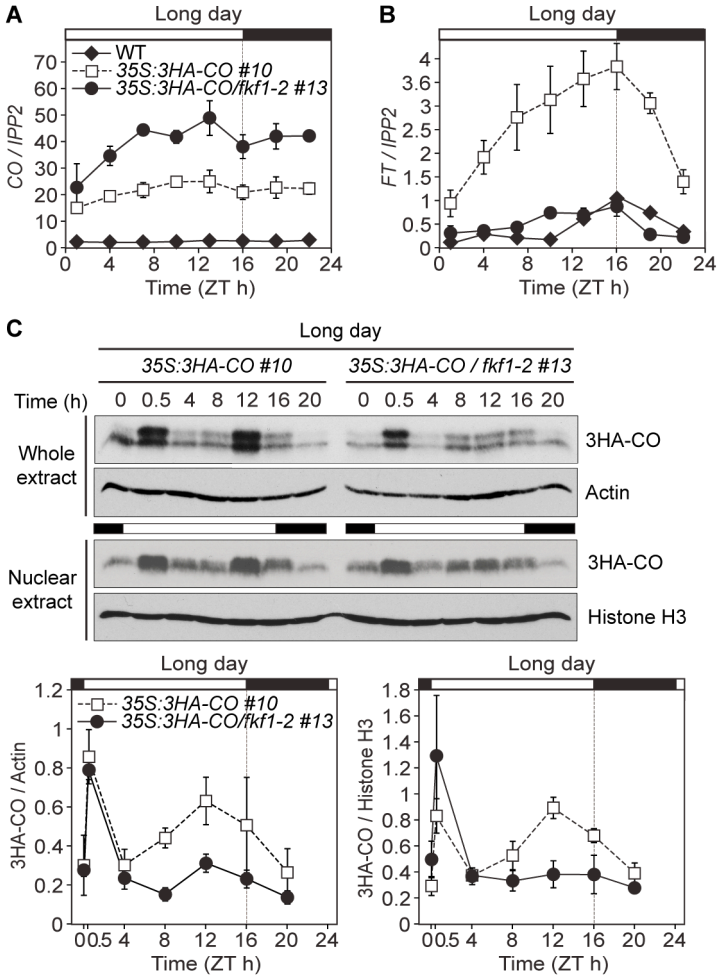

Fig. S6.
Diurnal patterns of CO protein expression in *35S:3HA-CO* plants. (**A** and **B**) Expression levels of *CO* (**A**) and *FT* (**B**) mRNA in WT, *35S:3HA-CO #10* line, and *35S:3HA-CO/fkf1-2 #13* line under long-day conditions. The results are means ± SEM from three biological replicates. (**C**) Daily oscillation of CO protein abundance in the *35S:3HA-CO #10* and the *35S:3HA-CO/fkf1-2 #13* lines under long-day conditions. Plants were harvested on day 10 at indicated time points and used for isolation of whole and nuclear extract. Actin and histone H3 proteins were used for internal controls in whole and nuclear extracts, respectively. The levels of CO protein were quantified using NightOwl imaging system.

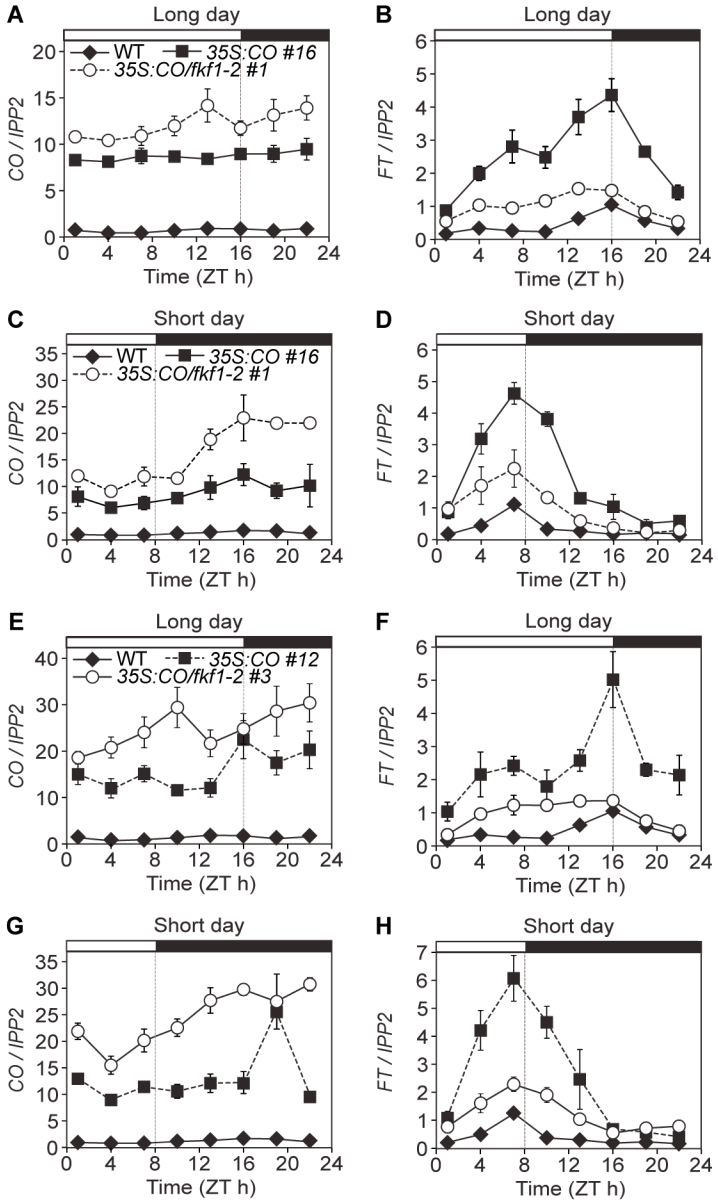

Fig. S7.
The expression levels of *CO* and *FT* mRNA in wild type, *35S:CO*, and *35S:CO/fkf1-2* plants in long days and short days. Two independent transgenic lines, in which the amounts of *CO* expression were different, were generated in wild type or *fkf1-2* background. Seedlings were grown for 10 days in long days (**A**, **B**, **E**, and **F**) and short days (**C**, **D**, **G**, and **H**). Q-PCR was carried out using three independently harvested samples. The mRNA levels of *CO* (**A**, **C**, **E**, and **G**) and *FT* (**B**, **D**, **F**, and **H**) were normalized against *IPP2* expression.

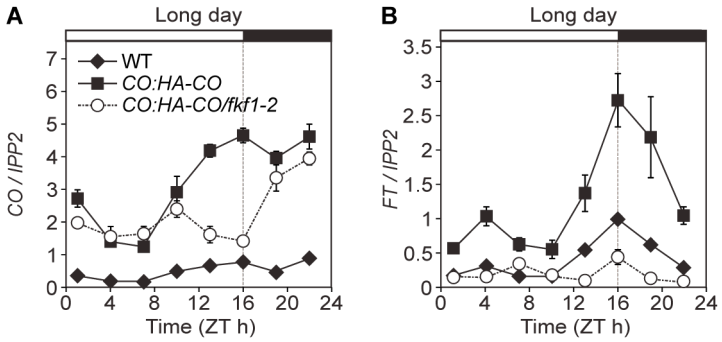

Fig. S8.
The expression levels of *CO* and *FT* mRNA in wild type, *CO:HA-CO*, and *CO:HA-CO/fkf1-2* plants in long days. (**A** and **B**) In the *CO:HA-CO* transgenic line, *CO* mRNA levels were elevated in the tissue where *CO* is usually expressed. The *CO:HA-CO/fkf1-2* line was generated by genetic cross between the *CO:HA-CO* and *fkf1-2* plants. Wild type, *CO:HA-CO*, and *CO:HA-CO/fkf1-2* were grown in long days and harvested at day 10. The daytime *CO* mRNA expression levels in the *CO:HA-CO/fkf1-2* line were lower than in the parental *CO:HA-CO* line. This is most likely due to the fact that stabilized CDF proteins directly repressed *CO* transcription (*9, 10, 14*). However, the *CO* mRNA levels in the *CO:HA-CO/fkf1-2* plants were still higher than in wild type plants. Even though *CO* levels in the *CO:HA-CO/fkf1-2* plants were higher, *FT* mRNA levels were lower than in wild type plants. These results indicate that FKF1 is involved in activation for both *CO* and *FT* transcription. Q-PCR was carried out using three independently harvested samples. The mRNA levels of *CO* (**A**) and *FT* (**B**) were normalized against *IPP2* expression.

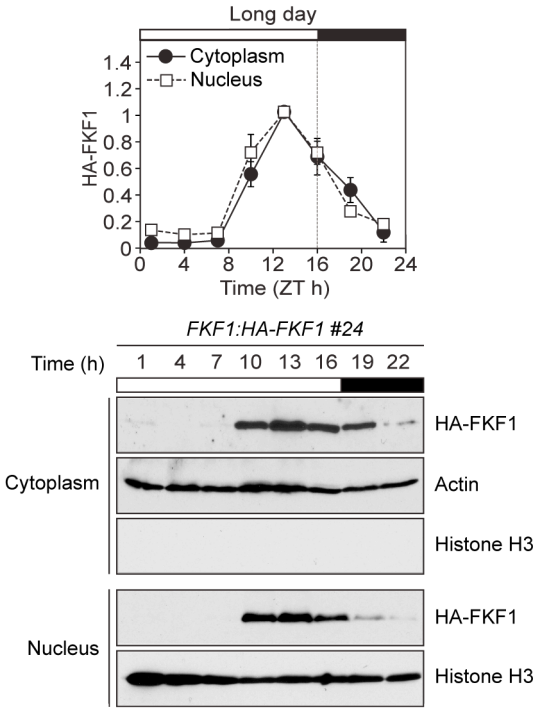

Fig. S9.
FKF1 protein exists in both cytoplasm and nucleus. *FKF1:HA-FKF1/fkf1 #24* plants were grown in long days and harvested at day 10. Approximately 0.5 g of ground tissues were suspended in 1X nuclei isolation buffer (CelLytic Plant Nuclei Isolation/Extraction Kit, Sigma) and cleared by a filter mesh (CelLytic Plant Nuclei Isolation/Extraction Kit, Sigma). After centrifugation, the supernatant was used as cytoplasmic proteins and the pellet was used to further extract nuclei for nuclear proteins. Amounts of cytoplasmic and nuclear FKF1 proteins were normalized against actin and histone H3 proteins, respectively. The experiments were repeated three times with biological replicates.

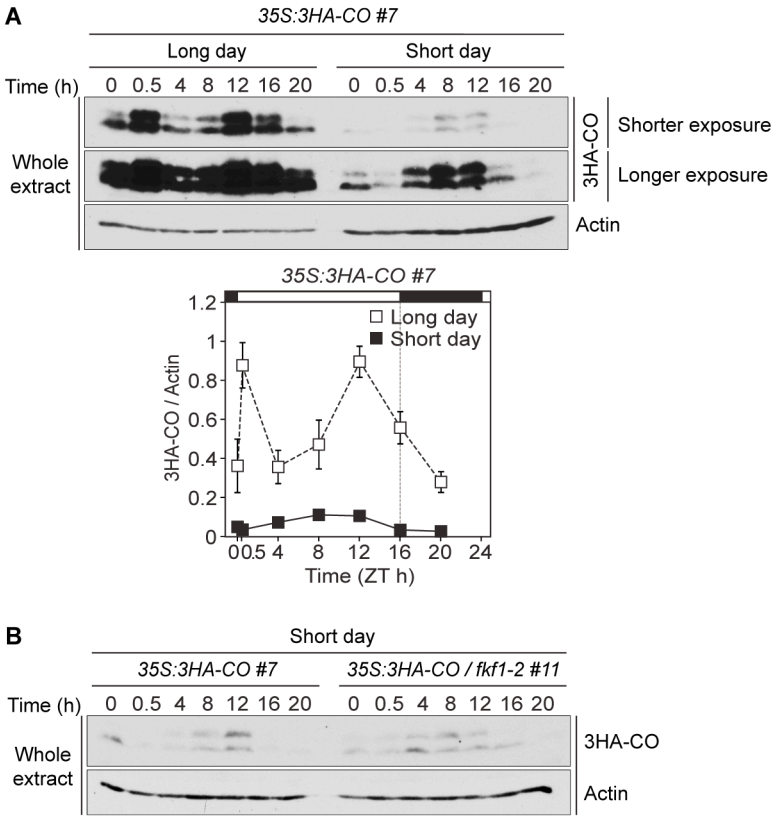

Fig. S10.
Diurnal patterns of CO protein in *35S:3HA-CO* plants under short-day conditions. (**A**) Relative expression levels of CO protein in the *35S:3HA-CO #7* line in long days and short days. Proteins were visualized by western blot (upper panel) and quantified by the imaging system (lower panel). (**B**) The levels of CO protein in the *35S:3HA-CO #7* and the *35S:3HA-CO/fkf1-2 #11* lines under short-day conditions.

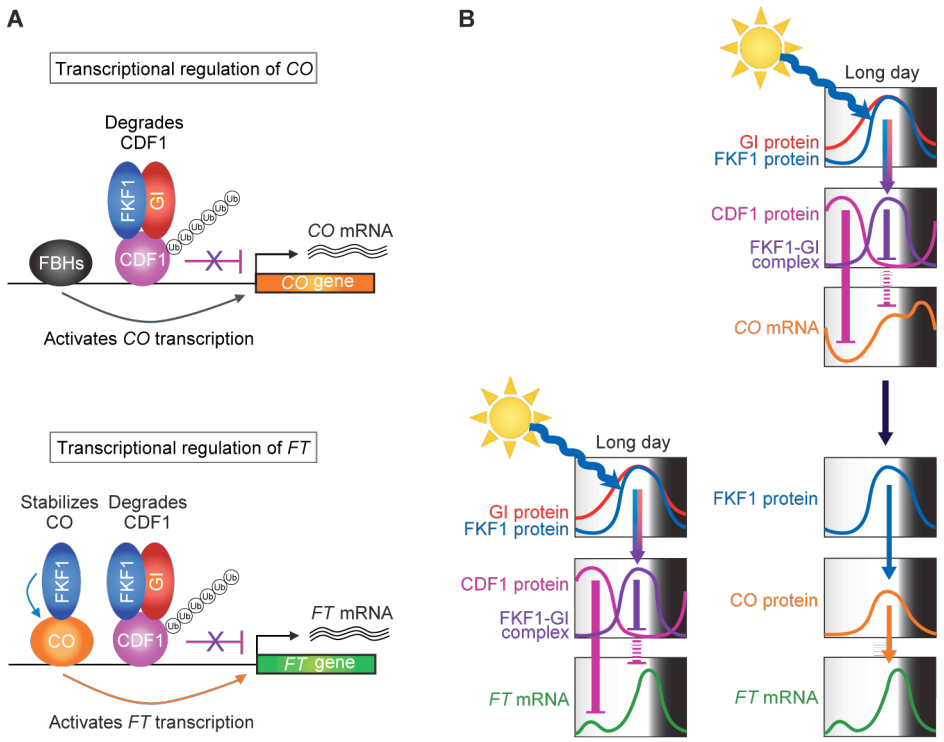

Fig. S11.
A model of FKF1-dependent *FT* regulation. (**A**) Schematic representation of FKF1-dependent *CO* and *FT* transcriptional regulation. CDF1 and possibly other CDF proteins bind to the *CO* promoter and repress *CO* transcription. FKF1 interacts with GI in long days, and the FKF1-GI complex degrades CDF proteins. When the FKF1-GI complex removes CDF-dependent repression from *CO* transcription, FLOWERING BHLH (FBH) proteins activate *CO* transcription through direct association with the *CO* promoter (*40*). CDF proteins also repress *FT* expression by binding to the *FT* promoter. The FKF1-GI complex removes CDF proteins from the *FT* promoter. Simultaneously, CO protein is stabilized by FKF1 in a blue-light dependent manner and activates *FT* transcription. (**B**) Temporal regulation of *FT* expression by FKF1 functions. In long days, light-activated FKF1 forms a complex with GI in the afternoon, then the FKF1-GI complex releases CDF1 repression on the *CO* promoter by degradation of CDF1 protein, which allows *CO* mRNA to be expressed in the late afternoon (upper panel). The same CDF1 degradation mechanism by the FKF1-GI complex is present on the *FT* promoter (left of lower panel), which enables *FT* expression to be induced in the afternoon. FKF1 is also involved in stabilization of CO protein. When FKF1 is expressed in the afternoon, CO protein is stabilized by FKF1 (right of lower panel). Both degradation of CDF1 on the *FT* promoter by the FKF1-GI complex and stabilization of CO by FKF1 facilitate the induction of *FT* expression by CO protein in the later afternoon (lower panel). Since the timing of *FKF1* expression is regulated by the circadian clock and because FKF1 function is regulated by blue light, the long-day afternoon is the only time that FKF1 function is fully activated.

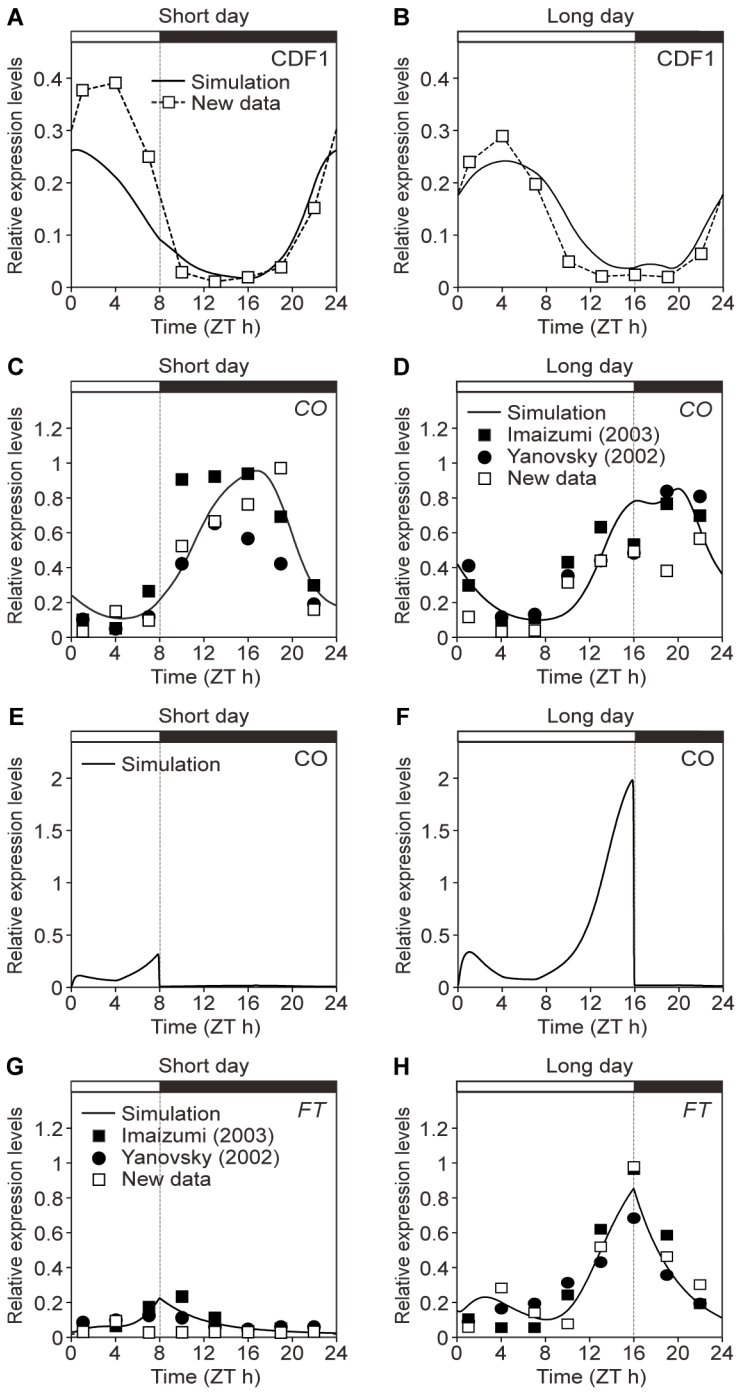

Fig. S12.
Model simulations compared to wild type data. Simulations of CDF1 protein (**A** and **B**), *CO* mRNA (**C** and **D**), CO protein (**E** and **F**), and *FT* mRNA (**G** and **H**) are plotted in short-day (**A**, **C**, **E**, and **G**) and long-day (**B**, **D**, **F**, and **H**) conditions. Data from this study and Salazar *et al.* (*11*) have been included to show the match of the model where possible.

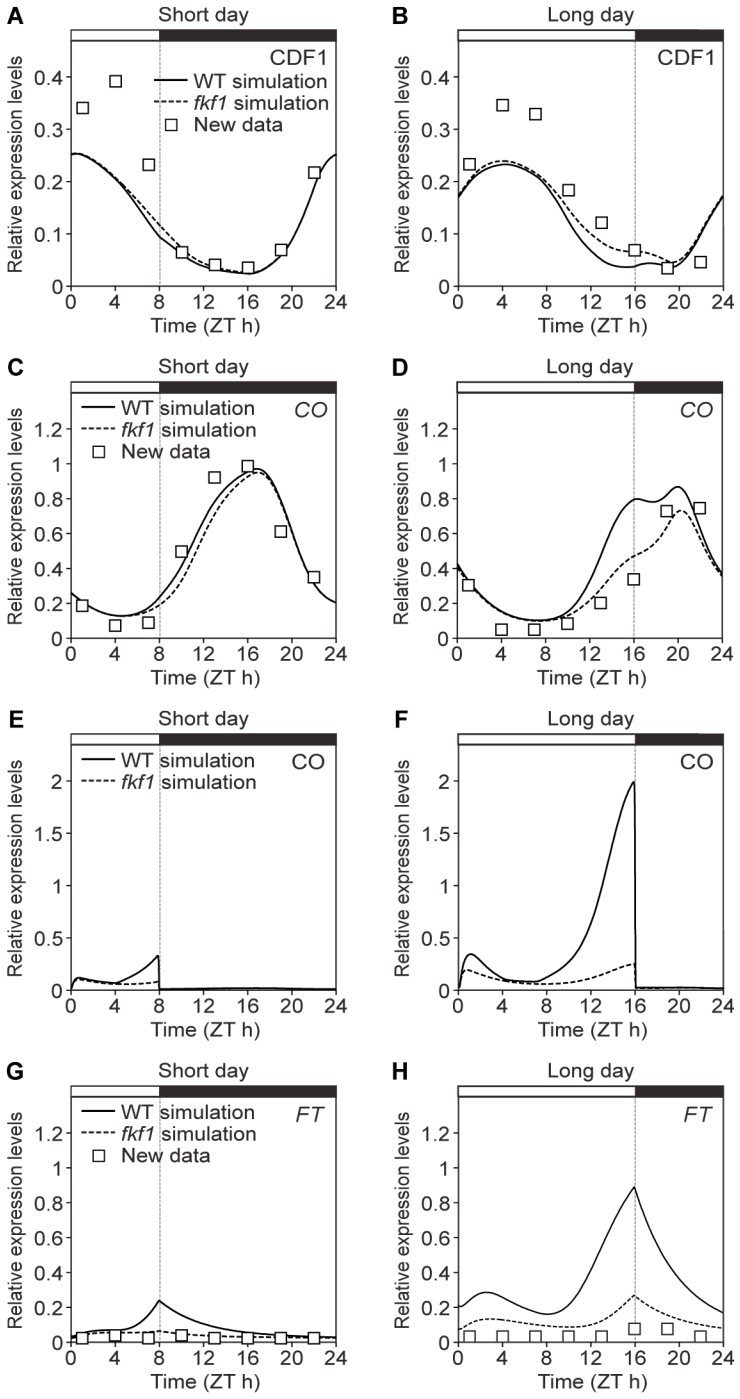

Fig. S13.
Simulations of *fkf1* mutant. As in fig. S12, components of the model are simulated in wild type and *fkf1* mutant backgrounds and compared to data (*8*).

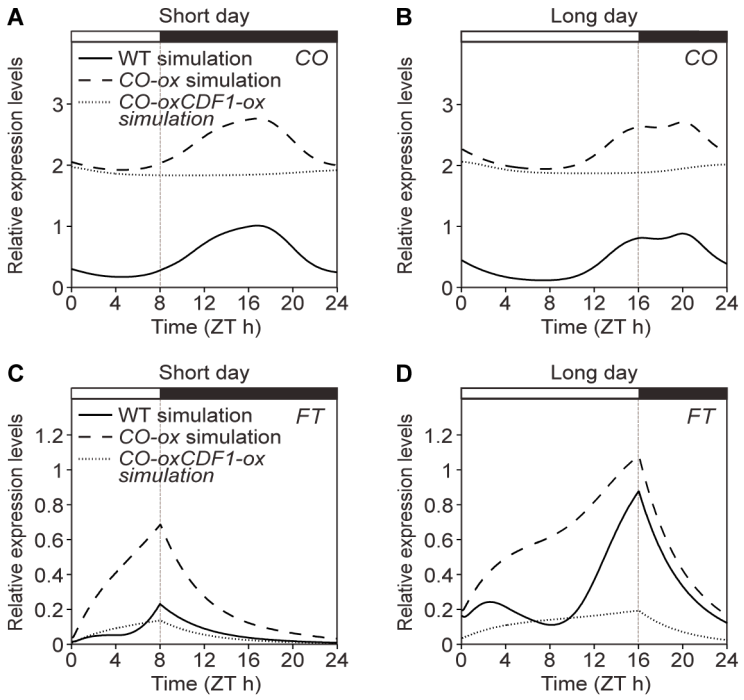

Fig. S14.
Simulations of *CO* overexpressor and *CDF1* and *CO* overexpression lines. *CO* (**A** and **B**) and *FT* (**C** and **D**) mRNA are simulated in short day (**A** and **C**) and long day (**B** and **D**) conditions in wild type, *CO*-ox, and *CO*-ox/*CDF1*-ox backgrounds. The simulations can be qualitatively compared to data in Fig. 1.

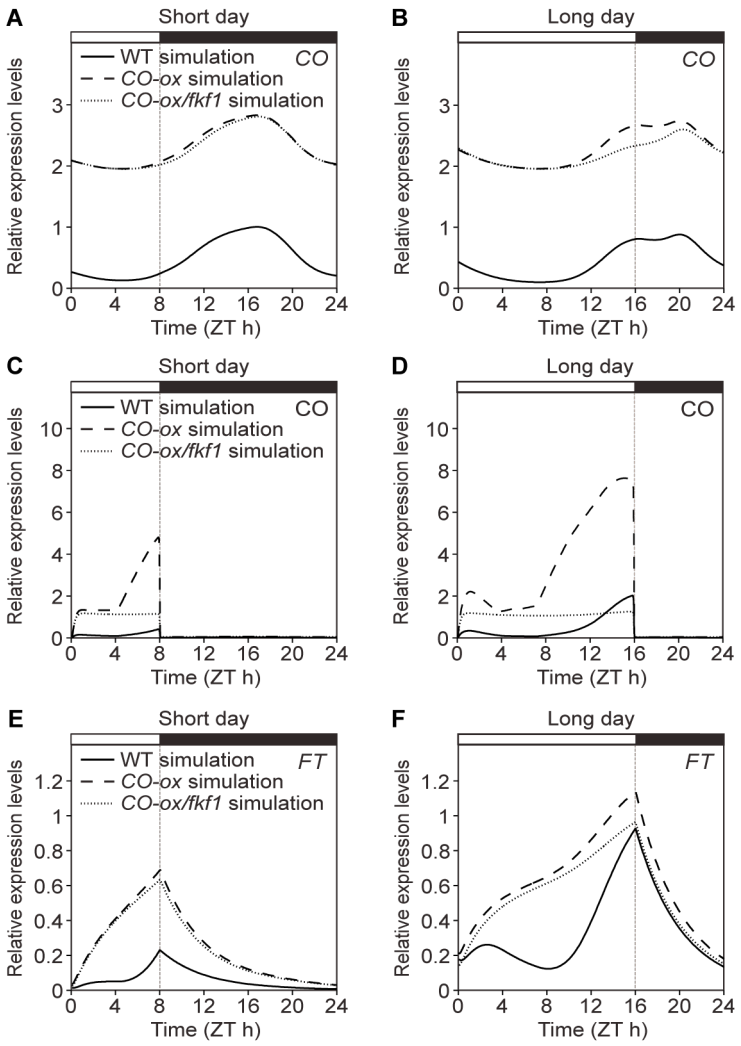

Fig. S15.
Simulations of *CO* overexpressor and *CO*-ox/*fkf1* mutants. As in fig. S12, components of the model are simulated in wild type, *CO*-ox, and *CO*-ox/*fkf1* mutant backgrounds. The simulations of (**B**, **D**, and **F**) can be compared to data in Fig. 3.

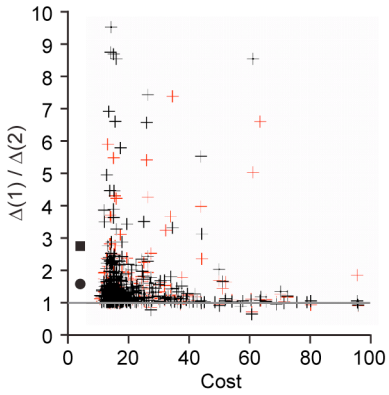

Fig. S16.
Random parameter sets selected to match the data show that *FT* mRNA levels are more affected by CO stabilization than CDF1 degradation. 500 quasi-random sets of parameter values were scored for the fit of the resulting simulations to the training data, as described in the Supplementary Information. Partial mutants Δ(1) and Δ(2) were simulated with each parameter set, as in Fig. 4D, to test whether CO stabilization or CDF1 degradation had most effect on *FT* levels. For Δ(1) and Δ(2) simulated from each parameter set, FT_{AREA}^{LD} (red +) or the maximum expression level of wild type long-day *FT* (black +) were calculated. The total cost for simulations with each random parameter set against all the training data (*CO* and *FT* mRNAs, and CDF1 protein) is plotted (x-axis) against the ratio of phenotypic effects in Δ(1) and Δ(2) partial mutants. The ratio of FT_{AREA}^{LD} (circle) and the maximum level of expression (square) for the original parameter set are shown as reference points. The grey line represents Δ(1) effect = Δ(2) effect. Points above the line (Δ(1) effect > Δ(2) effect) indicate a greater effect on *FT* transcription from CO stabilization than from CDF1 degradation.

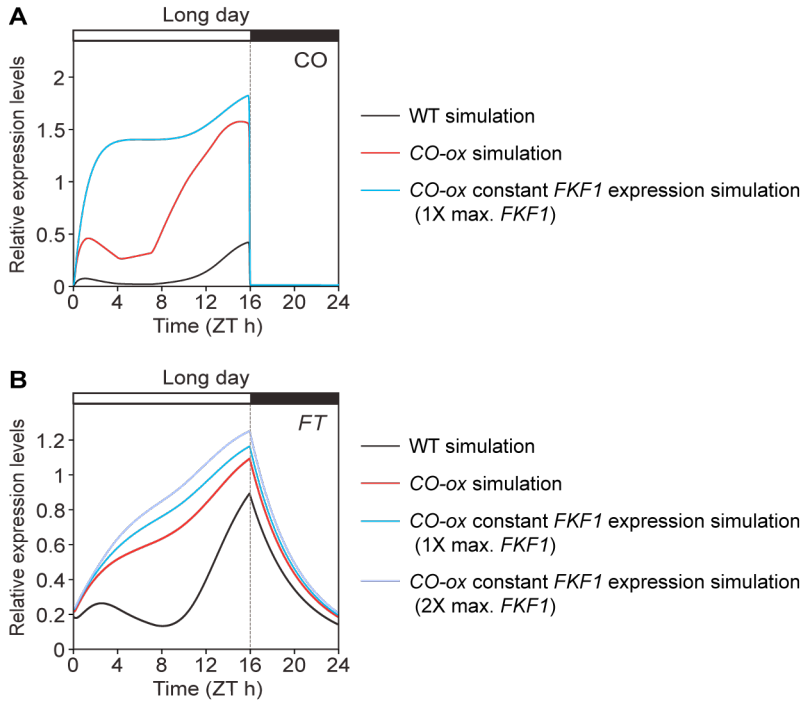

Fig. S17.
Predicted effect of constitutively expressed *FKF1* on CO protein stabilization and *FT* mRNA profiles. (**A**) Comparison of simulations of CO protein profiles in WT, *CO*-ox, and *CO*-ox/*FKF1*-ox lines. The effects of *FKF1* constitutive expression (1X max.: same as the peak WT *FKF1* mRNA level) on the CO protein regulation were calculated. (**B**) Comparison of simulations of long day *FT* mRNA in WT, *CO-ox*, and two *CO-ox/FKF1-ox* lines. The effects of two levels of *FKF1* constitutive expression on the *FT* mRNA profiles were calculated. (1X max.: same as the peak WT *FKF1* mRNA level, and 2X max.: double the maximum level of WT *FKF1* mRNA)

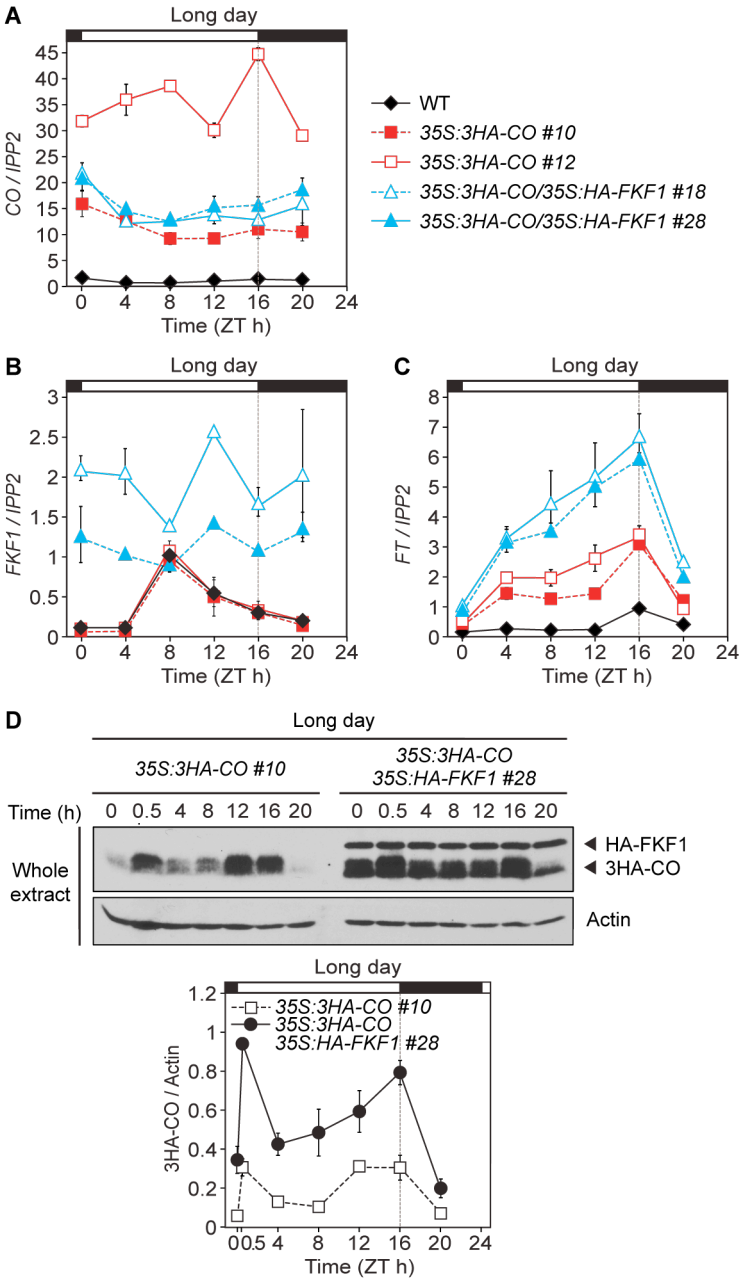

Fig. S18.
Effect of constitutively expressed *FKF1* on CO protein stabilization and *FT* mRNA expression. Wild type, *35S:3HA-CO* lines, and *35S:3HA-CO/35S:HA-FKF1* lines were grown in long days and harvested on day 10. (**A** to **C**) The mRNA levels of *CO* (**A**), *FKF1* (**B**), and *FT* (**C**) were normalized against *IPP2* expression. *CO* mRNA levels in the double overexpressors were higher than those in the *35S:3HA-CO #10* but lower than those in the *35S:3HA-CO #12* plants (**A**). The levels of *FKF1* mRNA expression was varied between two double overexpressors; *FKF1* mRNA in the *35S:3HA-CO/35S:HA-FKF1 #28* line was constantly expressed as the WT peak level, and *FKF1* expression levels in *35S:3HA-CO/35S:HA-FKF1 #18* were higher than the other (**B**). *FKF1*

expression levels in these lines similarly match the conditions of simulations shown in fig. S17. The *35S:3HA-CO/35S:HA-FKF1 #28* represents 1X max. *FKF1* line and *#18* represents 2X max. *FKF1* line. Although the levels of *CO* mRNA in the double overexpressors were lower than in *35S:3HA-CO #12*, *FT* mRNA levels were higher than the *CO* overexpressor with a WT background (**C**), validating the computational prediction shown in fig. S17. (**D**) Western blot analysis showed that CO proteins were stabilized when *FKF1* is constantly expressed. A representative X-ray file image is shown in the upper panel. Actin proteins were used for internal controls. The levels of CO protein were quantified using the NightOwl imaging system (lower panel). The results are means ± SEM from three independent biological replicates. These results indicate that FKF1 function on CO protein stabilization is important to regulate *FT* transcription.

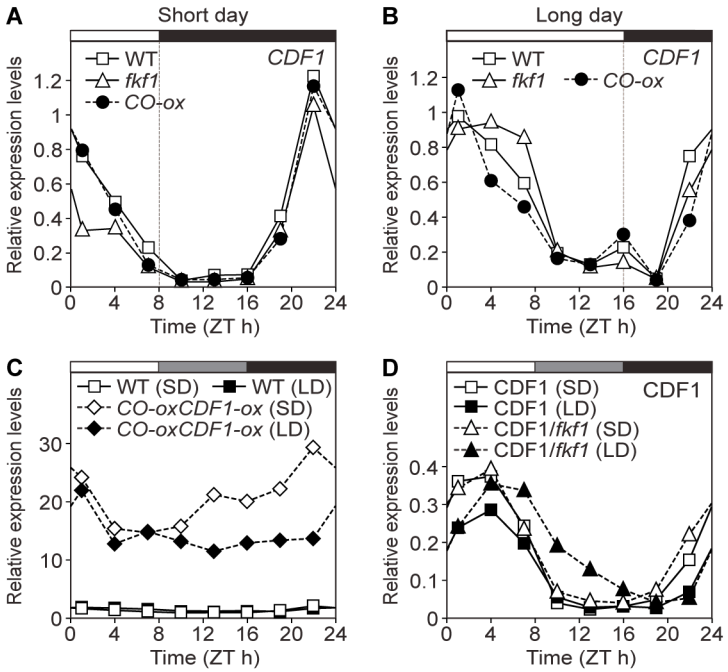

Fig. S19.
CDF1 mRNA and protein data. (**A** and **B**) *CDF1* mRNA is relatively unchanged in wild type, *fkf1*, and *CO* overexpressor backgrounds in both short days (**A**) and long days (**B**). (**C**) *CDF1* mRNA is greatly increased in *SUC2:CO-HA/35S:CDF1* background. (**D**) In long days, CDF1 protein is increased at dusk in *fkf1* mutants compared to wild type. Closed symbols represent long day (LD) data, open symbols represent short day (SD) data.

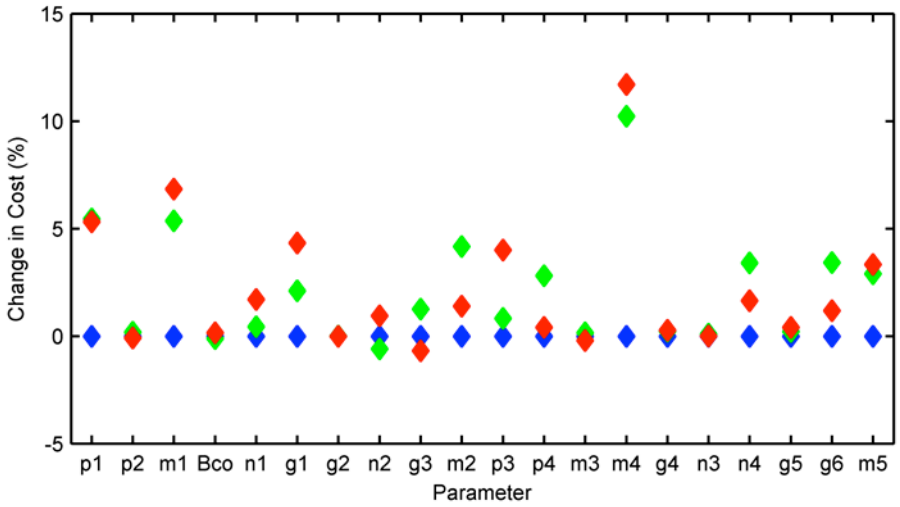

Fig. S20.
Parameter sensitivity analysis illustrates the robustness of the model to single parameter changes. The model parameters (represented by blue diamonds) were increased (green diamonds) and decreased (red diamonds) by 10% of their original value. The percentage change in the cost of wild type *FT* simulations under long days is recorded. Cost decreases correspond to better-fitting simulations.

Table S1.
Parameter values.

Parameter	Interpretation	Value	Units
p_1	*CDF1* mRNA translation	0.09825	1/hr
p_2	Rate of GI/FKF1-dependent CDF1 degradation	7.74706	1/hr
m_1	Rate of GI/FKF1-independent CDF1 degradation	0.3344	1/hr
B_{CO}	Basal *CO* transcription	0.049	nM/hr
n_1	Maximum rate of CDF1-dependent *CO* transcription	4.33	1/hr
g_1	Michaelis-Menten coefficient for CDF1 inhibition of *CO*	0.055	
a	Hill coefficient	2	
g_2	Michaelis-Menten coefficient for FKF1-independent GI disruption of CDF1 activity	0.00005	
n_2	Maximum rate of CDF1-independent *CO* transcription	1.365	1/hr
g_3	Michaelis-Menten coefficient for activation of *CO*	2	
b	Hill coefficient	2	
m_2	*CO* mRNA degradation	0.864	1/hr
p_3	*CO* mRNA translation	0.564125	1/hr
p_4	Rate of CO stabilization by FKF1	4.4484	1/hr
m_3	Basal CO protein degradation	38.3384	
m_4	Dark-dependent CO protein degradation	1.0851	
g_4	Michaelis-Menten coefficient for FKF1-CO stabilization	0.1	
n_3	CDF1-independent *FT* transcription	0.135	1/hr
n_4	CDF1-dependent *FT* transcription	1.546	1/hr
g_5	Michaelis-Menten coefficient for CDF1 inhibition of *FT*	0.165	
g_6	Michaelis-Menten coefficient for CO activation of *FT*	0.276	
c	Hill coefficient	2	
m_5	*FT* mRNA degradation	0.243	1/hr

Supporting references

1. B. Thomas, D. Vince-Prue, *Photoperiodism in plants* (Academic Press, San Diego, ed. 2, 1997).
2. Y. Kobayashi, D. Weigel, *Genes Dev* **21**, 2371 (2007).
3. A. de Montaigu, R. Toth, G. Coupland, *Trends Genet* **26**, 296 (2010).
4. R. Amasino, *Plant J* **61**, 1001 (2010).
5. A. Samach *et al.*, *Science* **288**, 1613 (2000).
6. F. Valverde *et al.*, *Science* **303**, 1003 (2004).
7. T. Mockler *et al.*, *Proc Natl Acad Sci U S A* **100**, 2140 (2003).
8. T. Imaizumi, H. G. Tran, T. E. Swartz, W. R. Briggs, S. A. Kay, *Nature* **426**, 302 (2003).
9. T. Imaizumi, T. F. Schultz, F. G. Harmon, L. A. Ho, S. A. Kay, *Science* **309**, 293 (2005).
10. M. Sawa, D. A. Nusinow, S. A. Kay, T. Imaizumi, *Science* **318**, 261 (2007).
11. J. D. Salazar *et al.*, *Cell* **139**, 1170 (2009).
12. Y. Fukamatsu *et al.*, *Plant Cell Physiol* **46**, 1340 (2005).
13. M. Sawa, S. A. Kay, *Proc Natl Acad Sci U S A* **108**, 11698 (2011).
14. F. Fornara *et al.*, *Dev Cell* **17**, 75 (2009).
15. See details in materials and methods that are available as supporting material on *Science* Online.
16. L. Q. Han, M. Mason, E. P. Risseeuw, W. L. Crosby, D. E. Somers, *Plant J* **40**, 291 (2004).
17. Z. Zuo, H. Liu, B. Liu, X. Liu, C. Lin, *Curr Biol* **21**, 841 (2011).
18. S. B. Tiwari *et al.*, *New Phytol* **187**, 57 (2010).
19. U. Alon, *Nat Rev Genet* **8**, 450 (2007).
20. Y. H. Song, I. Lee, S. Y. Lee, T. Imaizumi, J. C. Hong, *Plant J* **69**, 332 (2012).
21. M. Karimi, D. Inze, A. Depicker, *Trends Plant Sci* **7**, 193 (2002).
22. J. C. Carrington, D. D. Freed, A. J. Leinicke, *Plant Cell* **3**, 953 (1991).
23. P. Hajdukiewicz, Z. Svab, P. Maliga, *Plant Mol Biol* **25**, 989 (1994).
24. J. S. Rohila, M. Chen, R. Cerny, M. E. Fromm, *Plant J* **38**, 172 (2004).
25. A. Baudry *et al.*, *Plant Cell*, (2010).

26. N. Nakamichi *et al.*, *Plant Cell Physiol* **48**, 822 (2007).
27. Y. Niwa *et al.*, *Plant Cell Physiol* **48**, 925 (2007).
28. C. Bowler *et al.*, *Plant J* **39**, 776 (2004).
29. M. J. Yanovsky, S. A. Kay, *Nature* **419**, 308 (2002).
30. J. C. Locke *et al.*, *Mol Syst Biol* **1**, 2005 0013 (2005).
31. S. Laubinger *et al.*, *Development* **133**, 3213 (2006).
32. S. Jang *et al.*, *Embo J* **27**, 1277 (2008).
33. L. J. Liu *et al.*, *Plant Cell* **20**, 292 (2008).
34. H. Wang, L. G. Ma, J. M. Li, H. Y. Zhao, X. W. Deng, *Science* **294**, 154 (2001).
35. B. Liu, Z. Zuo, H. Liu, X. Liu, C. Lin, *Genes Dev* **25**, 1029 (2011).
36. C. S. Pittendrigh, *Cold Spring Harb Symp Quant Biol*, 159 (1960).
37. P. Suarez-Lopez *et al.*, *Nature* **410**, 1116 (2001).
38. M. Ashyraliyev, Y. Fomekong-Nanfack, J. A. Kaandorp, J. G. Blom, *FEBS J* **276**, 886 (2009).
39. A. Pokhilko *et al.*, *J Theor Biol* **270**, 31 (2011).
40. S. Ito *et al.*, *Proc Natl Acad Sci U S A* **109**, 3582 (2012).